Chemical Engineering Journal, Volume 336, 15 March 2018, Pages 211-222
DOI:10.1016/j.cej.2017.11.128

# Mechanism of deoxygenation in anisole decomposition over single-metal loaded HZSM-5: Experimental study

Jiajun Zhang[a, b], Beatriz Fidalgo[b], Athanasios Kolios[b], Dekui Shen[a,]*, Sai Gu[c]

* Corresponding author: D.S., e-mail address: 101011398@seu.edu.cn

[a] Key Laboratory of Energy Thermal Conversion and Control of Ministry of Education, Southeast University, Nanjing, China

[b] School of Water, Energy and Environment, Cranfield University, Cranfield, United Kingdom

[c] Faculty of Engineering and Physical Sciences, University of Surrey, Surrey, United Kingdom

## Abstract[1]

This work investigates the deoxygenation reaction during the decomposition of anisole (methoxy-rich model compound of lignin) over bi-functional catalyst. The bi-functional catalyst consisted of a single metal loaded on an acid support; the active metals, i.e. Ni, Co, Mo and Cu, were loaded at various rates, and the acid support was HZSM-5 zeolite with a Si/Al ratio of 25 (HZ(25)). Experiments were conducted in a bench-scale fluidised bed reactor within the temperature range from 400˚C to 600˚C. Experimental results revealed that the increase in temperature and metal loading promoted the selectivity of BTX fraction. Nevertheless, a simultaneous increase in the yield of carbonaceous deposits was also observed at the expense of liquid fraction, both phenolics compounds (Phs) and aromatic hydrocarbons (AHs). 500˚C was the preferred temperature for BTX production. Ni-loaded HZ(25) catalyst

[1] Abbreviations: HZ(25), HZSM-5 with Si/Al ratio of 25; x%M/HZ(25), x% metal M loaded HZ(25); BTX, benzene, toluene and xylene; AH, aromatic hydrocarbon; Phs, phenolic compounds

Published by Elsevier. This is the Author Accepted Manuscript issued with: Creative Commons Attribution Non-Commercial No Derivatives License (CC:BY:NC:ND 4.0). The final published version (version of record) is available online at DOI:10.1016/j.cej.2017.11.128. Please refer to any applicable publisher terms of use.

could dramatically facilitate the conversion of Phs to monoaromatics and increase the selectivity of BTX fraction by 43.4%; Mo-loaded HZ(25) catalyst exhibited the best catalytic activity towards the total production of AHs and promoted the BTX yield by 27.1%. It was also found that 1 wt.% was the optimum loading ratio for both Ni and Mo on HZ(25) to obtain the highest BTX yield and selectivity. Characterization of fresh bi-functional catalysts showed that micro polycrystalline metal sites, in the range of 4 -10 nm, existed on the fresh catalyst and exhibited strong interaction with the HZ(25) support. For the spent catalysts, large amount of amorphous carbonaceous deposit was observed, ascribed to the polycondensation of aromatic compounds during the reaction. Three reaction pathways were proposed for the catalytic deoxygenation of anisole, with the hydrogen being available in-situ as product of the polycondensation reactions.

**Key words**: anisole; catalytic decomposition; deoxygenation; bi-functional catalyst; BTX

## 1. Introduction

Large amount of waste lignin is produced annually by the pulp and paper industry [1–3]. Conversion of lignin into a liquid fraction via fast pyrolysis, followed by the catalytic upgrading of this fraction is a promising approach to produce aromatic hydrocarbons that can be used as additives for transport fuel, such as the BTX fraction, i.e. benzene, toluene, and xylene [4–6]. Methoxy compounds abundantly exist in the primary liquid product derived from fast pyrolysis of lignin; and the catalytic deoxygenation is a favourable route for their upgrading for fuel application [7]. Anisole (or methoxybenzene) is a prototype model compound to investigate the reactivity of methoxyl-based lignin-derived compounds [8]. The decomposition of anisole is commonly recognized to consist of two steps: transmethylation and deoxygenation [9–11]. Transmethylation is considered to be the initial reaction step of the process; it mainly produces methyl-containing Phs, which are intermediates for

the subsequent formation of AHs [12–16]. Further conversion of the Phs through deoxygenation reaction at higher temperature gives rise to AHs and even naphthenic hydrocarbons [9–11].

Metal-based solid catalysts are one of the most promising catalysts used in lignin fast pyrolysis and the upgrading of the derived bio-oil to produce AHs [11,17,18]. These catalysts consist of active metals dispersed on a solid support. Various supports have been studied, including inert metal oxides (i.e. $SiO_2$, $Al_2O_3$ etc.), carbon nanofibers, and acid zeolite (i.e. HBeta, HZSM-5 etc.) [19], with the latter being most widely used [20–23]. Transition metals, such as Ni, Co, Mo and Pt etc., have been found to be highly active catalysts for product reforming [20,24–26]. The use of noble metals as catalysts for the lignin derived bio-oil upgrading and catalytic reforming have been widely investigated using representative model compounds [23,27,28]. Metal-supported solid catalysts promote the deoxygenation reactions during the decomposition of anisole; and noble metals, especially Pt, has been reported to exhibit good catalytic performance in such process [20,29]. However, the applicability of noble metals is hindered by their high costs. The use of base metals has been suggested as they are preferred in terms of lower cost. However, regardless the increasing interest of using base metals in catalytic fast pyrolysis of lignin and its related model compounds [17,26,30–35], anisole decomposition over base metal based catalysts have been rarely reported.

It is commonly acknowledged that acid sites play an important role in anisole decomposition [36–38]. Nevertheless, limited literature reporting the use of bi-functional catalyst, i.e. consisting of a base metal and acid solid support, in the decomposition of anisole is available. On the other hand, most of the research work about deoxygenation stage in the catalytic anisole decomposition considers the external supply of hydrogen to the reaction atmosphere [20,24,39–42]. The use of hydrogen not only increases the cost and risk of the process, but also an excessive

hydrogen supply normally leads to aromatic ring saturation with high selectivity towards cyclohexane and cyclohexanol [40]. There is an increasing interest in using alternative hydrogen sources, such as hydrogen-rich AH mixtures (propylene, n-decane, benzene, or tetralin) [13]. Nevertheless, there is a lack of investigations that evaluate the ability of in-situ hydrogen supply during the reaction of anisole decomposition; even though the methyl group in the anisole molecule is a hydrogen-rich group itself.

In this work, the catalytic deoxygenation reaction during the decomposition of anisole, as a lignin-related model compound, was investigated. Bi-functional catalysts, consisting of a single metal (i.e. Ni, Co, Mo and Cu) loaded on acid support (HZSM-5 zeolite with a Si/Al ratio = 25) were used. The effect of temperature and metal loading on quantity and quality of the products was studied. Experiments were performed in a bench-scale fluidised bed reactor under atmosphere pressure to investigate the intrinsic reaction mechanism.

## 2. Materials and methods

### 2.1. Materials

Anisole was supplied by Aladdin Reagents Co., Ltd. The HZSM-5 (Si/Al=25, HZ(25)) zeolite catalyst was provided by Nankai University Catalyst Co., Ltd, China. Precursors of metal active site used for catalyst synthesis, i.e. nickel nitrite hexahydrate ($Ni(NO_3)_2 \cdot 6H_2O$), cobalt nitrite hexahydrate ($Co(NO_3)_2 \cdot 6H_2O$), ammonium molybdate tetrahydrate ($(NH_4)_6Mo_7O_{24}.4H_2O$), and copper nitrate trihydrate ($Cu(NO_3)_2 \cdot 3H_2O$), were supplied by Aladdin Reagents Co., Ltd. The chemicals used for calibration in GC-MS (analytical purity) were also provided by Aladdin Reagents Co., Ltd. $N_2$, $H_2$ and all the standard gaseous species used for the operation and calibration of GC-FID were supplied by Nanjing Shangyuan Industrial Gas Plant at a purity of 99.999%.

## 2.2. Methods

### 2.2.1. Catalyst preparation

Single metal/HZ(25) catalysts were synthesized by wet impregnation of the support (HZ(25)) with aqueous solutions of the metal precursor, i.e. $Ni(NO_3)_2 \cdot 6H_2O$, $Co(NO_3)_2 \cdot 6H_2O$, $(NH4)_6Mo_7O_{24}.4H_2O$ and $Cu(NO_3)_2 \cdot 3H_2O$, in different concentrations depending on the targeted active metal loading (see supplementary file S1 for full details). The impregnation mixtures were stirred with a magnetic stirrer during 24 h at room temperature (~25°C). Water was removed by evaporation at 80°C and the impregnated support was then dried at 110°C for 12 h, followed by air calcination in a muffle furnace at 500°C for 6 h. The calcined catalyst precursors were crushed and sieved to a particle size range between 60-80 mesh. The catalysts were reduced in-situ with 25 vol.% $H_2/N_2$ (total flow rate of 500 mL/min) for 2 h before each experiment. Reduction temperatures were established from $H_2$-TPR analyses and varied with the loaded metal. Catalysts with various metal loadings were prepared, i.e. 0.5, 1 and 5 wt.% in the case of Ni and Mo, and 1 wt.% in the case of Co and Cu. Catalysts were denoted as x%M/HZ(25), where M is the active metal (M = Ni, Cu, Mo or Co) and x is the loading ratio (x = 0.5, 1, or 5).

### 2.2.2. Catalyst characterization

#### 2.2.2.1 $H_2$-TPR

$H_2$-TPR (Temperature Programmed Reduction) analyses were performed on the calcined impregnated supports to determine the reduction temperature for the metal active sites. About 100 mg of the sample was loaded in a U-shaped quartz tube and flushed with a 20 mL/min Ar stream at 400°C for 40min. The temperature was then decreased to room temperature (~25°C) under inert conditions. The sample was reduced under a stream of 10 vol.% $H_2$/Ar (total flow rate of 20 mL/min) with the temperature increasing at a heating rate of 10°C/min up to 800°C. The output signal of $H_2$ concentration was detected with a thermal conductive detector (TCD).

#### 2.2.2.2 TEM-EDS

Both fresh (reduced) and spent metal-based HZ(25) catalysts were analyzed by Transmission Electron Microscopy (TEM) in order to evaluate the morphology of metal active sites and carbonaceous deposits on the zeolite support. Specimens were prepared by ultrasonic dispersion of catalyst samples in ethanol before dropping the suspension to a copper/nickel grid. A Tecnai G2 T20 provided by FEI Ltd was used. Images of the microstructure and the relevant selected area electron diffraction (SAED) patterns of the specimens were acquired. Energy Dispersive Spectrometer (EDS) tests were also performed using Genesis 2000 from EDAX Ltd. to determine the elements present on the sample surface.

#### 2.2.2.3 XPS

X-ray photoelectron spectroscopy (XPS) tests were carried out to evaluate the surface composition of the fresh catalyst samples and the composition of carbonaceous deposits on the spent catalyst. The tests were performed in a XPS analyser ESCALAB 250Xi from Thermo Fisher Scientific Inc. with an Al Kα X-ray source (10 mA, 20 kV), under the conditions of 20 and 100 eV pass energy for the survey spectra and the single element spectra (Ni, Co, Mo, Cu, C), respectively. Peaks were identified by means of the American National Institute of Standards and Technology (NIST) database.

### 2.2.3 Experiments

Experiments were carried out in the bench scale fluidised bed reactor (D*H (mm) = 32*600) sketched in Fig. 1. Nitrogen was used as fluidising gas, and the flow velocity was adjusted by running cold experiments, and set to approximately two times the minimum fluidisation velocity, found to be $U_{mf}$ = 0.027 m/s. Details on the calculation of $U_{mf}$ are found elsewhere [10, 31].

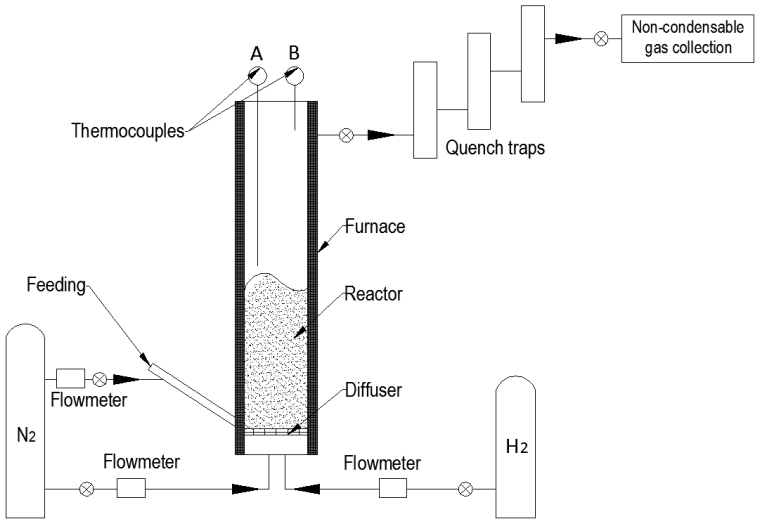


Fig. 1 Schematic for reactor setup

For each experiment, 50 g of fresh catalyst was placed inside the reactor and fluidised by a $N_2$ flow rate of 154 L/h. A total amount of 8.3 g of liquid anisole was place in a syringe pump at the beginning of the experiment and pumped into the reactor at a constant flow rate of 50 g/h during the test. Reaction time was 10 min. The effect of temperature was investigated performing catalytic decomposition experiments over 1%Ni/HZ(25) at 400, 500 and 600°C. In order to investigate the effect of the metal type on the anisole decomposition, experiments were carried out over 1%Ni/HZ(25), 1%Co/HZ(25), 1%Mo/HZ(25) and 1%Cu/HZ(25) at 500°C. The effect of metal loadings were investigated by performing experiments with 0.5%Ni/HZ(25), 1%Ni/HZ(25), 5%Ni/HZ(25), 0.5%Mo/HZ(25), 1%Mo/HZ(25) and 5%Mo/HZ(25) at 500°C. For each experiment, the outflow stream was passed through a three stages quench traps to collect the liquid product, which was further diluted to a constant volume of 150 mL. The liquid fraction was then analysed by GC-MS in an Agilent GC7890 gas chromatograph-mass spectrometer equipped with a capillary column DB-5ms (30 m x 250μm x 0.25μm). The injector temperature was kept at 270˚C. The column was programmed from 40˚C (3 minutes) to 180˚C (2 min) with the heating rate of 5˚C/min, and finally to 280°C (held 2 min) with the heating rate of 10°C/min. Overall running time for each GC-MS test was 45min. The mass

spectra were operated in electron ionization (EI) mode at 70 eV, and were obtained from m/z 35-550. Each species in the liquid sample were quantified by total ion and were identified based on the database of NIST library, and was calibrated with an external standard solvent. All detected compounds (peak threshold value: 18) were utilised for the calibration. The amount of carbonaceous deposits on the spent catalyst was determined by thermogravimetric analysis with a SETSYS-1750 CS Evolution TG Instrument. In each test, around 15 mg of sample was charge in the pan and heated from room temperature (~25°C) up to 900°C at a heating rate of 20 °C/min and under an air flow rate of 20 mL/min. The sample was kept at 900°C for 15 min to ensure total burn-out of the carbonaceous deposits. Non-condensable gaseous products were analysed by GC-FID, which was equipped with a column SE54. The injection volume of gaseous sample was 1µL, and the injector temperature was 270°C with 6.3 mL/min helium as the carrier gas. The initial column temperature was set to 40°C with equilibration time of 2 min, and the maximum temperature was 300°C. Overall running time for each GC-FID test was 45 min. Yields of the liquid fraction, carbon deposits and gaseous fraction were determined as a percentage of the initial weight of the anisole sample. The standard deviation of the liquid and carbonaceous deposit yields were evaluated by the repeating three sets of experiments; further details are provided in supplementary file S2.

# 3 Results and discussion

## 3.1 Characterization of fresh catalysts

The reduction temperature for each metal oxide loaded on HZ(25) was determined by $H_2$-TPR analyses. Fig. 2 shows the $H_2$-TPR profiles of Ni/HZ(25), Co/HZ(25), Mo/HZ(25) and Cu/HZ(25) catalyst samples. In the case of Ni/HZ(25) catalyst, two distinct peaks at around 423°C and 535°C were observed. The larger peak at 423°C indicates a higher consumption of hydrogen, which points to the principal reduction of NiO to Ni at this temperature. The second peak at 535°C relates to the metal oxides

in the channels of zeolite that are more difficult to reduce due to the stronger interaction between the metal sites and support, which may be attributed to the presence of acidic sites in the zeolite support [24,41,44,45]. The reduction profile of Co/HZ(25) also showed two peaks at around 516°C and 672°C respectively. The major peak is assigned to the transition of CoO to Co. The small peak evolved at higher temperature suggests the existence of nanosize CoO species in the zeolite channels and the stronger metal-support interaction [44,46]. In the case of Mo/HZ(25) catalyst, a main $H_2$ peak evolved at around 424°C, and a shoulder to that peak was observed at around 453°C, indicating the reduction of $MoO_3$ to $MoO_2$. Another peak at 710°C is attributed to further reduction of $MoO_2$ to metal Mo [47,48]. Two clearly distinctive reduction peaks were observed in the case of Cu/HZ(25) at 201°C and 425°C respectively. The first peak is assigned to the reduction of intra-zeolite CuO to $Cu_2O$, while the peak at higher temperature corresponds to the further reduction to Cu [45,49,50]. Besides, additional minor $H_2$ consumption was observed at 600°C, which is ascribed to the copper oxides particles in zeolite channels that are difficult to be reduced.

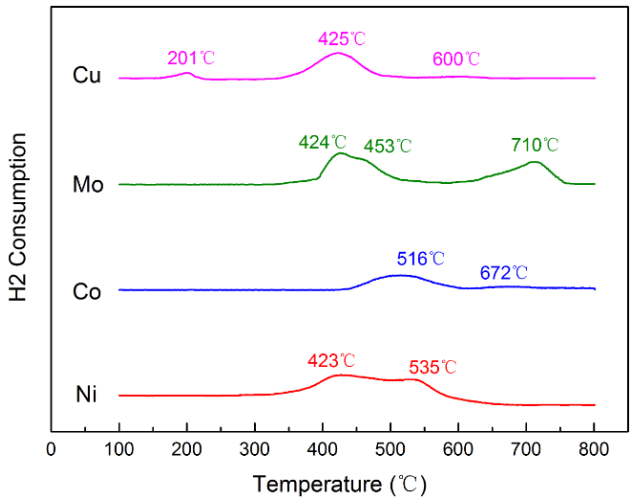


Fig. 2 $H_2$-TPR profiles of M/HZ(25) (with M = Ni, Co, Mo, or Cu). 10 vol.%$H_2$/Ar flow rate = 20mL/min; Heating rate = 10°C/min

Following $H_2$-TPR results, Ni/HZ(25) and Cu/HZ(25) were in-situ reduced at 600°C, Co/HZ(25) was reduced at 700°C, and Mo/HZ(25) was reduced at 800°C respectively prior to fresh catalysts characterization and experiment.

TEM analyses with various magnifications (200nm, 100nm, 50nm, and 20nm) were performed on fresh 1%M/HZ(25) samples, i.e. 1%Ni/HZ(25), 1%Co/HZ(25), 1%Mo/HZ(25), and 1%Cu/HZ(25). Representative TEM micrographs are shown in Fig. 3**,** and more graphs can be found in the supplemental files S6 to S9. For the four catalysts, the metal particles were observed to be highly dispersed on the zeolite surface in the form of primarily micro polycrystal [51,52]. The crystal nature was confirmed by the diffraction rings shown in the selected area electron diffraction (SAED) patterns (see supplementary files S6 to S9). Fig. 3 highlights the average sizes of the crystals for each catalyst, which were found to range between 4 and 10 nm for all metals. As it shown in Fig. 3 (a), the microcrystal particles of Ni exhibited irregular shape, and were difficult to be distinguished. Sankaranarayanan et al. [44] observed the same when evaluating Ni loading by TEM. The particles of Mo and Cu also consisted of microcrystals with blurry boundaries, as shown in Figs. 3 (c) and (d). On the contrary, the Co microcrystals showed polygon shapes with clear boundaries, as shown Fig. 3(b).

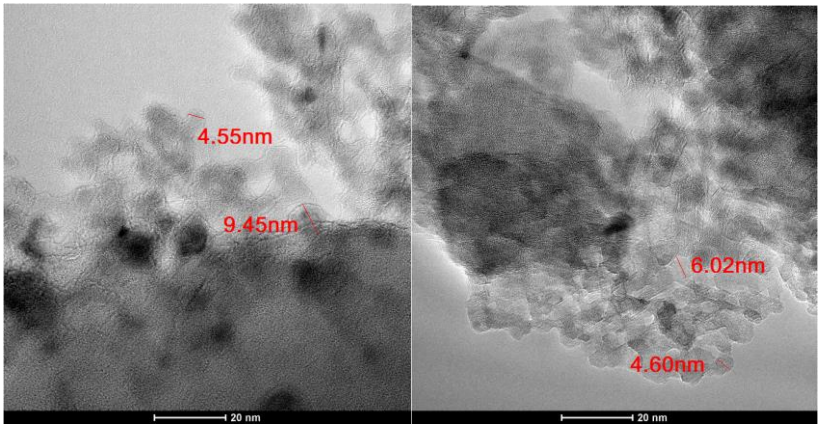


(a) (b)

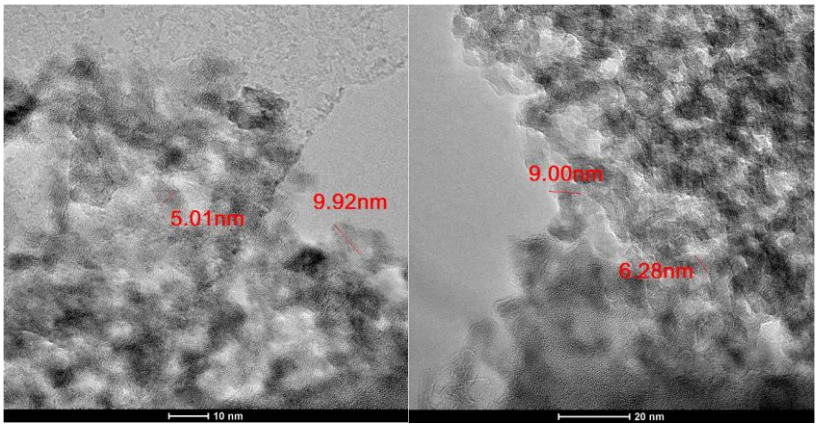


(c) (d)

Fig. 3 TEM micrographs of the fresh catalysts: (a) 1%Ni/HZ(25) , (b) 1%Co/HZ(25), (c) 1%Mo/HZ(25) and (d) 1%Cu/HZ(25)

EDS tests were carried out to confirm the main elements present in the surface of the four fresh catalysts and estimate their quantities, as shown in Table 1 and Supplementary file S3[2]. For each of the catalysts, the active metal species were found to be in a concentration around 1 wt.% (based on the whole catalyst sample weight), which agrees with the expected loading ratio.

Table 1 Metals loading on single metal loaded catalysts detected by EDS

| **Catalyst** | **Elem** | **Weight%** | **Atomic%** |
|---|---|---|---|
| **1%Ni/HZ(25)** | Ni | 1.0 | 0.3 |
| **1%Co/HZ(25)** | Co | 1.3 | 0.4 |
| **1%Mo/HZ(25)** | Mo | 1.1 | 0.2 |
| **1%Cu/HZ(25)** | Cu | 1.4 | 0.4 |

[2] Copper support grid was used for testing the Ni, Co, and Mo catalysts in the tests of TEM-EDS, and nickel support grid was used for testing the Cu catalysts. The net grid metals were also identified in the tests but have been excluded in the quantitative analysis.

XPS was used to identify the state (i.e. valence) of metal elements on the surface of the reduced fresh catalyst and evaluate the interaction between metals and the support. The spectra for fresh 1%Ni/HZ(25), 1%Co/HZ(25), 1%Mo/HZ(25) and 1%Cu/HZ(25) were based on Ni(2p), Co(2p), Mo(3d) and Cu(2p) respectively and shown in Fig. 4.

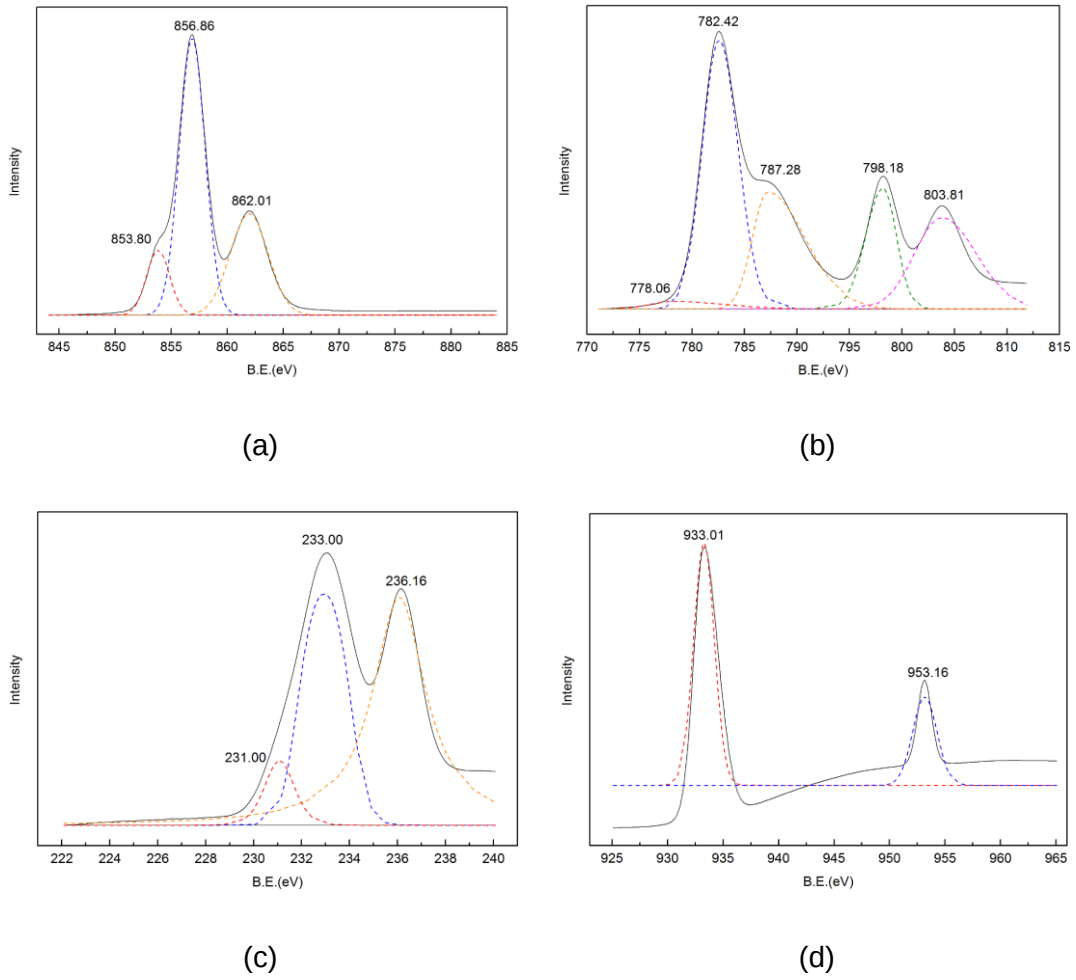


Fig. 4 XPS spectra of (a) Ni(2p) on Ni/HZ(25), (b) Co(2p) on Co/HZ(25), (c) Mo(3d) on Mo/HZ(25), (d) Cu(2p) on Cu/HZ(25)

For Ni/HZ(25), the peaks at 862.01 and 856.86 eV are ascribed to $Ni^{2+}$, which can be either $Ni(OH)_2$ or NiO, and the peak at 853.80 eV is assigned to $Ni^0$. In the case of Co/HZ(25), five peaks were identified; the first peak at 787.28 eV is assigned to CoO, and the peaks at 803.82, 798.18 and 782.42 eV can all be assigned to $Co(OH)_2$. The small peak at 778.06 eV is attributed to $Co^0$. In the case of Mo/HZ(25), the peaks at

236.16 and 233.00 eV are ascribed to MoOx, and the peak at 231.00 eV may attribute to either $Mo^0$ or $Mo(OH)_x$/Mo. For Cu/HZ(25), two peaks were seen. The peak at 953.16 eV can be assigned to either CuO or $Cu(OH)_2$, and the other peak at 933.01 eV is attributed to $Cu^0$.

XPS revealed that despite the catalysts were reduced under hydrogen at the required temperature, metals at different oxidization state are still found to different extent in all samples. This can be due to both unreduced metals and active metal sites interacting with the HZ(25) zeolite support, especially their connections to the structure oxygen. Considering that XPS is a surface technique and the surface metal would be readily reduced at the corresponding temperatures, the metal support interaction is expected to be the main reason. Similar phenomenon has been previously reported in the literature [53]. The metal hydroxides i.e. $Ni(OH)_2$, $Co(OH)_2$, $Mo(OH)_x$ and $Cu(OH)_2$ are regarded as the evidence for the interactions between the metal and acid sites. The results in Fig. 4 also show that the oxidised state was dominating in the case of Ni/HZ(25), Co/HZ(25), and Mo/HZ(25); particularly in Co/HZ(25) sample where only a small portion of $Co^0$ was observed [54–56]. On the contrary, relatively large amount of $Cu^0$ was detected in Cu/HZ(25), which implies that Cu may have less interaction with the HZ(25) support compared to the other metals. This is in agreement with the $H_2$-TPR results that showed lower reduction temperatures for Cu/HZ(25) catalyst compared to the other metal-based catalyst; no obvious interaction peak was observed at temperatures higher than 450°C.

### 3.2 Effect of temperature on deoxygenation reaction over single metal/HZ(25) catalysts

The effect of temperature on deoxygenation reaction in the anisole decomposition process over 1%Ni/HZ(25) was evaluated within 400°C and 600°C (experiments D1, D2 and D3 in Table 2). The anisole conversion and yields of liquid, gas and solid (carbonaceous deposits) products are shown in Table 2. The conversion of anisole

was 90.0% at 400°C and 100% at both 500°C and 600°C. The total liquid product yield decreased with temperature from 41.6 wt.% at 400°C (excluding undecomposed anisole) to 19.9 wt.% at 600°C. On the contrary, the carbonaceous deposit yield increased from 45.2 wt.% at 400°C to 77.3 wt.% at 600°C. Gas product yield was lower than 0.4 wt.% in all cases. GC-FID analyses revealed that the gas fraction was mainly composed of alkanes and olefins at all the temperatures (see Supplemental files S4). These compounds are probably produced from the release of methyl groups.

Fig. 5 shows the composition of the liquid product obtained over 1%Ni/HZ(25) at the different tested temperatures. The composition of the liquid product obtained over HZ(25) is included for comparison; more details can be found elsewhere [10]. The liquid fraction produced at 400°C consisted mainly of undecomposed anisole and Phs. It is worth noting that the conversion of anisole over Ni-based catalyst (90%) was lower than that over non-metal HZ(25) catalyst (~99.4%) [10]. This result may be attributed to the combined effect of the loss of acid sites on the solid support due to the metal loading, and the negligible activity of the metal sites at 400°C. The amount of Phs significantly decreased with temperature; particularly in the case of 1%Ni/HZ(25) with Phs reduced to 2.4 wt.% at 500 °C and no Phs detected at 600°C. On the contrary, the yield of AHs increased with temperature, with a maximum of 28.8 wt.% achieved at 500°C. At all temperatures, AHs consisted mainly of BTX, although a small proportion of polycyclic aromatic hydrocarbon (PAH), including naphthalene and methyl naphthalene, was observed (<3 wt.% in yield). The maximum BTX yield was also observed at 500°C (25.6 wt.%), although maximum selectivity was achieved at 600°C. In the case of HZ(25), the maximum BTX yield was observed at 600°C. This 100°C difference in the peak temperature points to the effect of Ni in lowering the activation energy required for the deoxygenation reaction during anisole decomposition. Therefore, the increase in temperature favoured the

production of BTX through the deoxygenation of Phs compounds, which are abundant intermediates produced from the transmethylation of anisole [10]. Results revealed that temperatures of 500°C or higher are required for the deoxygenation reactions over 1%Ni/HZ(25) to occur. However, an increase in temperature also resulted in an increase in carbonaceous deposit yield and decrease in total liquid yield, which indicates that temperature rise promoted the solid products formation. Deoxygenation and carbonaceous deposit formation are known to be competitive reactions over Ni-based catalysts, both are favoured by high temperatures [57]. A compromise between the effects of these two reactions is better achieved at 500°C, which is found to be the optimum temperature giving rise to the highest BTX yield although decreasing the selectivity. Additionally, it is worth noting that multi-methyl Phs (xylenols and trimethyl-methyl Phs) were only detected in the liquid products at 400°C. This result suggests that these compounds are more readily to be converted to AHs and carbonaceous deposit at higher temperatures than phenol and cresols.

1 ------

2 Table 2. Conversion, product recovery and product yields (in wt.% of reactant) from anisole decomposition over HZ(25) and x%M/HZ(25).

| No. | Catalyst | T ($^{o}$C) | Conversion (%) | Product recovery (%) | Liquid products | | | | | Gas yield | Solid yield |
|---|---|---|---|---|---|---|---|---|---|---|---|
| | | | | | Liquid yield | | | | BTX selectivity [b] (%) | | |
| | | | | | Total | Phs | AHs | BTX | | | |
| T1 [a] | HZ(25) | 400 | 99.4 | n.d. | 72.5[c] | 70.0 | 1.9 | 1.9 | 2.6 | n.d. | 27.0 |
| T2 [a] | HZ(25) | 500 | 100 | n.d. | 41.2 | 10.0 | 31.2 | 23.6 | 57.1 | n.d. | 42.0 |
| T3 [a] | HZ(25) | 600 | | n.d. | 33.5 | 0.0 | 33.5 | 27.3 | 81.5 | n.d. | 46.2 |
| D1 | 1%Ni /HZ(25) | 400 | 90 | 96.8 | 51.6[c] | 37.8 | 3.8 | 3.0 | 7.3 | 0.1 | 45.2 |
| D2 | | 500 | 100 | 99.4 | 31.3 | 2.4 | 28.8 | 25.6 | 81.9 | 0.2 | 68.0 |
| D3 | | 600 | | 97.6 | 19.9 | 0.0 | 19.9 | 19.4 | 97.6 | 0.4 | 77.3 |
| D4 | 0.5%Ni /HZ(25) | 500 | | 99.3 | 33.8 | 6.7 | 27.2 | 23.9 | 70.6 | 0.1 | 65.4 |

| | | | | | | | | | | |
|---|---|---|---|---|---|---|---|---|---|---|
| D5 | 5%Ni /HZ(25) | 500 | 95.0 | 4.3 | 0.0 | 4.3 | 4.3 | 98.7 | 1.2 | 89.5 |
| D6 | 1%Co /HZ(25) | 500 | 95.9 | 37.6 | 8.8 | 28.8 | 25.9 | 68.8 | 0.1 | 58.2 |
| D7 | 1%Mo /HZ(25) | 500 | 100.0 | 38.8 | 3.6 | 35.2 | 30.0 | 77.4 | 0.5 | 60.7 |
| D8 | 0.5%Mo/HZ(25) | 500 | 96.0 | 35.7 | 5.3 | 30.4 | 25.6 | 71.7 | 0.6 | 59.7 |
| D9 | 5%Mo /HZ(25) | 500 | 99.9 | 35.4 | 8.0 | 27.3 | 25.2 | 71.2 | 0.3 | 64.2 |
| D10 | 1%Cu /HZ(25) | 500 | 98.2 | 40.8 | 7.1 | 33.7 | 28.3 | 69.3 | 0.5 | 56.9 |

n.d. non-determined

[a] Data derived from previous study [10]

[b] Selectivity calculated with respect to the total liquid yield, included unreacted anisole

[c] The value considers unreacted anisole

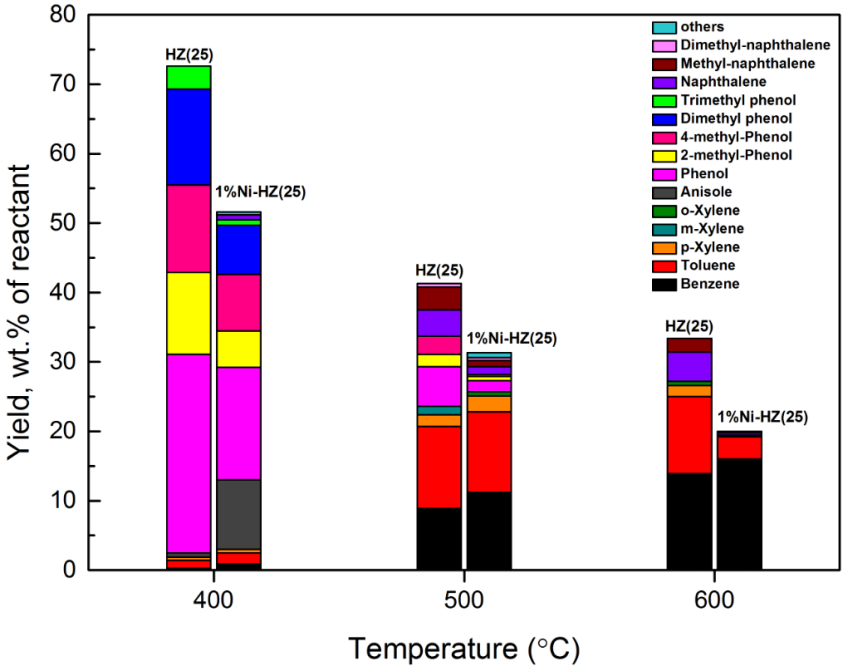


Fig. 5 Effect of temperature on the composition of the liquid product obtained from anisole decomposition 1%Ni/HZ(25) and HZ(25) (from reference [10]).

The lower conversion of anisole and total liquid yield observed over 1%Ni/HZ(25) catalysts compared to those over sole HZ(25) can be related to the larger formation of carbonaceous deposit caused by the 1 wt.% of Ni loading. Despite these lower values, both the BTX yield and selectivity improved when testing 1%Ni/HZ(25). The BTX yield increased from 1.9 wt.% to 3.0 wt.% at 400°C and from 23.6 wt.% to 25.6 wt.% at 500°C, although experienced a decrease from 27.3 wt.% to 19.4% at 600°C related to the higher yield of carbonaceous deposits. Simultaneously, the BTX selectivity enhanced from 2.6% to 7.3% at 400°C, from 57.1% to 81.9% at 500°C, and from 81.5% to 97.6% at 600°C. The results are attributed to more Phs being converted into BTX through deoxygenation and less polycyclic aromatic hydrocarbon (PAH) being formed in the presence of Ni active sites, especially at high temperatures. Nevertheless, at 400°C and 500°C, the significant decrease in the Phs yield over 1%Ni/HZ(25) compared to non-metal HZ(25) did not result in an equivalent increase in AHs yield, showing part of the Phs compounds were converted directly or indirectly, prior

formation of AHs, into carbonaceous deposit [36]. Indeed, the solid product fraction increased by respect 18.6 wt.% at 400°C and 26.0 wt.% at 500°C when using the Ni-based catalyst. Interestingly, the distribution of Phs products (cresols, xylenols and trimethyl-phenols) showed little change, which suggests that Ni sites did not inhibit the transmethylation reactions, and phenol, cresols and multi-methyl Phs formed during transmethylation were further consumed as the precursors for both AHs and carbonaceous deposit. Regardless the catalysts, no Phs were detected in the liquid product at 600°. Nevertheless, the BTX yield was lower over 1%Ni/HZ(25), which confirms that the severe formation of carbonaceous deposit on the Ni-based catalyst surface occurred at the expense of AHs. The higher BTX selectivity at 600°C achieved over 1%Ni/HZ(25) compared to HZ(25) points that the presence of Ni favours the production of monocyclic AHs by deoxygenation even at high temperature.

### 3.3 Effect of type of metal on deoxygenation reaction over single metal/HZ(25) catalysts

Four different metal-based catalysts were tested to evaluate the influence of the type of metal active site on the anisole conversion and yields products. Table 2 shows the experimental results obtained over 1%Ni/HZ(25) (D2), 1%Co/HZ(25) (D6), 1%Mo/HZ(25) (D7) and 1%Cu/HZ(25) (D10). Fig. 6 exhibits the liquid product distribution obtained over each of the metal-based catalysts at 500°C; results achieved with HZ(25) are also shown for comparison. Gas fraction composition is found in the Supplemental file S4. Metal-based catalysts lead to lower liquid yield and higher carbonaceous yield compared to non-metal catalyst. The lowest liquid yield of 31.3 wt.% and highest carbonaceous deposit yield of 68.0 wt.% were obtained over 1%Ni/HZ(25), while the highest liquid yield of 40.8 wt.% and the lowest carbonaceous deposit yield of 56.9 wt.% were obtained over 1%Cu/HZ(25). The results indicate that

Ni active site presents higher activity towards carbonaceous deposit formation than other metal sites at similar loading values.

Liquid products obtained from the experiments with 1%Mo/HZ(25) presented similar distribution to that for non-metal HZ(25). However, the Phs yield decreased significantly when the metal active site was added. The largest decrease was observed over 1%Ni/HZ(25) and 1%Mo/HZ(25). Regarding AHs, yield was improved from 31.2 wt.% to 35.2 wt.% when using 1%Mo/HZ(25), and to 33.7 wt.% when using 1%Cu/HZ(25). Similar AHs yield of 28.8 wt.% was observed over 1%Ni/HZ(25) and 1%Co/HZ(25) catalysts. Regardless the active metal, BTX constituted the main fraction of the AHs compounds. The BTX yield in the experiment with 1%Mo/HZ(25) was found to be the highest with a value of 30.0 wt.%, and a selectivity of 77.4% referred to the total liquid products. The rest of the liquid fraction consisted of PAH (yield of 5.2 wt.%) and Phs (yield of 3.6 wt.%). A lower BTX yield was achieved over 1%Ni/HZ(25), although this catalyst led to the highest BTX selectivity of 81%. A similar BTX yield was obtained with 1%Co/HZ(25). However, BTX selectivity was only 68.8%, mainly because of the lower conversion of Phs, as the PAH yield was relatively low (2.92 wt.%). In the case of 1%Cu/HZ(25), the liquid products consisted of 28.3 wt.% of BTX, with a selectivity of 69.3% due to a large proportion of both Phs (for 7.1 wt.%) and PAH (for 5.4 wt.%) formed.

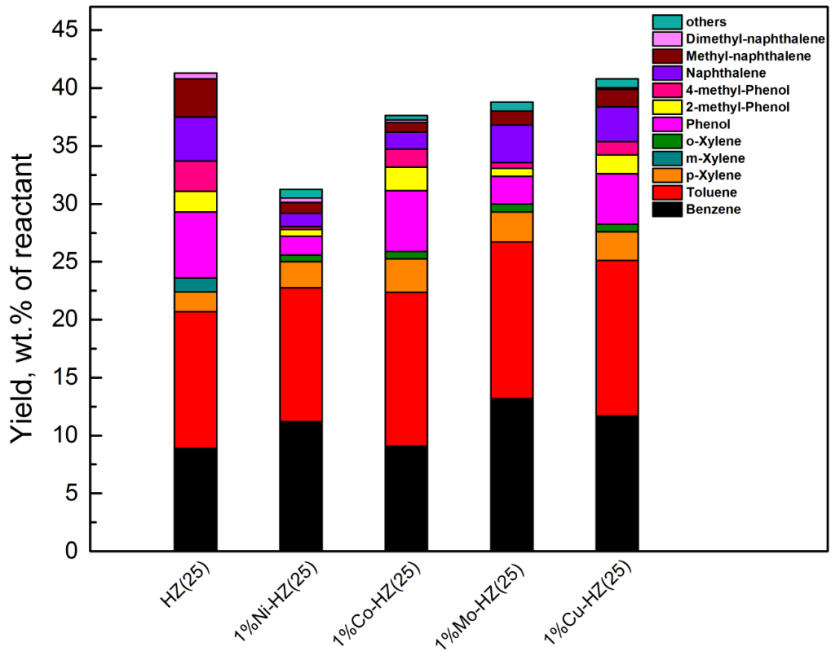


Fig. 6 Effect of type of metal on the composition of the liquid product obtained from anisole decomposition over 1%M/HZ(25) (M = Ni, Co, Mo or Cu) and HZ(25). Reaction temperature = 500 °C

Ni and Mo based catalysts exhibited distinctive performance respectively in BTX production among the four metal based catalysts in this study. Ni-based catalyst was observed to give rise to very high BTX selectivity in the liquid products, but it also promoted the formation of carbonaceous deposit resulting in a lower amount of total liquid product. Mo-based catalysts gave rise to higher yield of AHs compared to Ni-based catalysts, preserving more liquid products from being converted into carbonaceous deposits. However, it showed lower activity towards the conversion of Phs into AHs, and more formation of PAH, which decreased selectivity. It is hypothesized that a combination of Ni and Mo as bi-metal loading in one catalyst would integrate both effects; this hypothesis will be investigated in a future work of our group.

### 3.4 Effect of metal loading on deoxygenation reaction over single metal/HZ(25) catalysts

Three metal loadings, i.e. 0.5 wt.%, 1.0 wt.% and 5.0 wt.%, on catalysts of x%Ni/HZ(25) and x%Mo/HZ(25) were tested for the decomposition of anisole at 500°C (experiments D2, D4, D5 and D7, D8, D9 in Table 2). These two metals were selected based on the positive results shown in section 3.3. The anisole conversion and yields of liquid, gas and carbonaceous solid products are shown in Table 2, and the liquid yield distribution is exhibited in Fig. 7 (a) and (b).

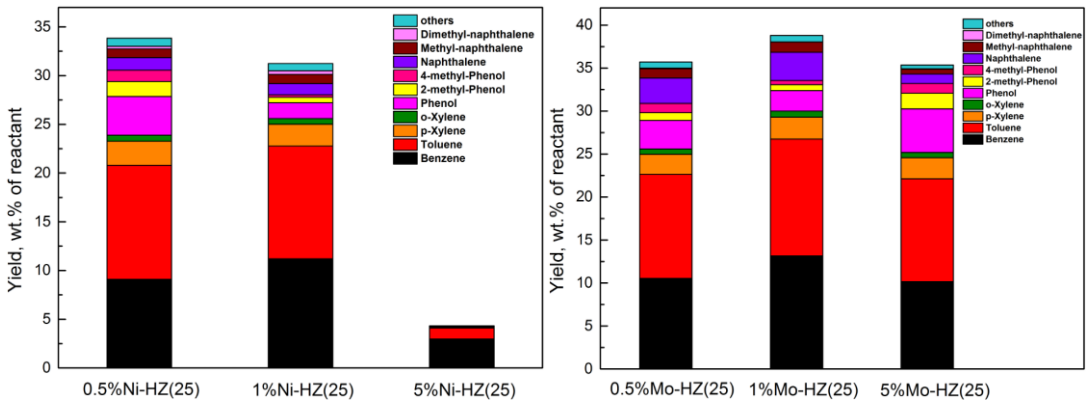


(a) (b)

Fig. 7 Effect of metal loading on the composition of the liquid product obtained from anisole decomposition: (a) x%Ni/HZ(25) catalyst and (b) x%Mo/HZ(25) catalyst, x = 0.5 wt.%, 1 wt.% and 5 wt.%. Reaction temperature = 500 °C

In the case of the catalyst series x%Ni/HZ(25), the increase in metal loading gave rise to a significant decrease in the total yield of liquid products, from 33.8 wt.% for 0.5%Ni/HZ(25) to 4.3 wt.% for 5%Ni/HZ(25). Accordingly, carbonaceous deposits increased from 65.4 wt.% to 89.5 wt.%. Gas product yields lower that 1.2 wt.% were obtained during these experiments reactions (composition of this fraction given in Supplemental file S4). Specifically, Phs yield was 6.7 wt.% when 0.5%Ni/HZ(25) was used, and decreased when the loading ratio increased, till no Phs were obtained in the

experiment with 5%Ni/based catalyst. The yields of AHs and BTX both experienced a slight rise when the loading ratio increased from 0.5 to 1wt.%, although they sharply deceased over 5%Ni/HZ(25) catalyst. Regarding BTX selectivity, it kept increasing with the loading ratio till 98.7% corresponding to the 5%Ni loading.

The results indicate that 0.5%Ni and 1%Ni loadings have similar catalytic activity towards the conversion of anisole into liquids. However, it seems that the conversion pathway of Phs into BTX is relatively impaired when using 0.5%Ni/HZ(25), and as a result the BTX selectivity for 1%Ni loading was higher than that for 0.5%Ni loading by 11.3%. Complete conversion of Phs into BTX was observed over 5%Ni/HZ(25) with almost 100% selectivity. This result confirms the high efficiency of Ni in production of monocyclic AHs. On the other hand, more solid products were found at the expense of liquid products when the loading ratio raised to 5 wt.%, which proves that Ni loading is also the key factor leading to the formation of carbonaceous deposit. Among the tested catalysts, 1%Ni/HZ(25) gave rise to the best results in terms of both BTX yield and selectivity, and carbonaceous deposits formation.

In the case of x%Mo/HZ(25) series, the differences in liquid yield and distribution due to increase of metal loading were not as significant as those observed with the x%Ni/HZ(25) series, particularly when referring to 5 wt.% loading. The maximum AHs yield, BTX yield and BTX selectivity were 35.2 wt.%, 30.0 wt.% and 77.4% respectively when using 1%Mo/HZ(25) as catalyst. At the same time, this catalyst exhibited a minimum for the Phs yield. This result indicates the increase of Mo loading may improve Phs conversion, but 5%Mo loading may be high enough for the metal sites to block the microspores of HZ(25) (atomic radius of Mo is ~2.0Å) and reduce the activity of the catalyst toward the formation of AHs to some extent [58]. Contrary to x%Ni/HZ(25) series, the increment of Mo loading did not affect significantly the production of carbonaceous deposits. This implies that Mo active sites are prone to

promote liquid formation even at high metal loading ratio. 1 wt.% loading of Mo gave rise to higher BTX yields than the other loading ratios, and the yield was also higher than that obtained over 1%Ni/HZ(25). However, none of the x%Mo/HZ(25) catalysts led to a BTX selectivity as high as that achieved over 1%Ni/HZ(25).

### 3.5 Characterization of spent catalysts

Carbonaceous deposits from on the spent catalyst samples 1%Ni/HZ(25), from experiment D2, and 1%Mo/HZ(25), from experiment D7, were characterised by TEM-EDS and XPS analyses. TEM micrographs are shown in Fig. 8. Comparing to the micrographs from the fresh catalysts (Figs. 3 (a) and (c)), it can be observed that carbonaceous deposits covered the catalyst surface after the reaction, such that the metal particles were almost non-visible. The absence of diffraction rings in Fast Fourier Transform (FFT) images of the spent catalyst confirms the amorphous nature of the carbon deposit (see Supplemental files S10 and S11).

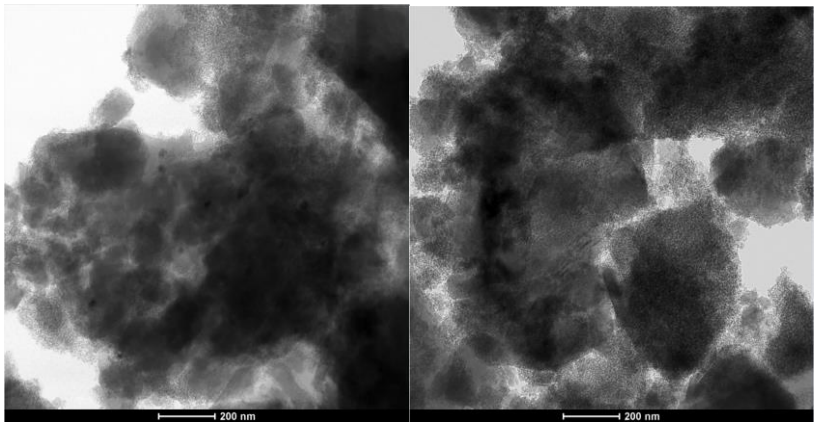


(a) (b)

Fig. 8 TEM micrographs for the spent catalysts: (a) 1%Ni/HZ(25) after experiment D2 and (b)1%Mo/HZ(25) after experiment D7

EDS tests were used to identify the main elements present in the surface of the spent catalysts and to estimate the amount of carbonaceous deposits, as shown and Table 3

(further details found in Supplemental file in S5). As can be seen, carbon element in the spent catalysts was roughly 6.6 wt.% for the spent 1%Ni/HZ(25) catalyst sample, and 5.0 wt.% for the spent 1%Mo/HZ(25) catalyst sample. This result agrees with the experimental results which showed that Ni-based catalysts gave rise to more carbonaceous products.

Table 3 Carbonaceous deposits on spent catalysts, 1%Ni/HZ(25) after experiment D2 and 1%Mo/HZ(25) after experiment D7, detected by EDS

| | Spent 1%Ni/HZ(25) | | Spent 1%Mo/HZ(25) | |
|---|---|---|---|---|
| Elem | Weight% | Atomic% | Weight% | Atomic% |
| C | 6.6 | 10.7 | 5.0 | 8.7 |
| Ni | 1.0 | 0.3 | - | - |
| Mo | - | - | 1.6 | 0.4 |

XPS spectra based on C(1s) for the spent catalysts are shown in Fig. 9. The samples were obtained from the experiments running over 1%Ni/HZ(25) at 400, 500 and 600°C (experiments D1, D2 and D3 respectively), and 1%Co/HZ(25), 1%Mo/HZ(25) and 1%Cu/HZ(25) at 500°C (experiments D6, D7 and D10, respectively). Carbon spectra from all spent catalysts exhibited three peaks, except in the case of 1%Mo/HZ(25) that exhibited only two obvious peaks.

The peaks around 289.10, 288.90 and 288.70 eV are assigned to chain compounds containing carbonyl groups, i.e.-$CH_2$-$C(CH_3)(C(O)O$-$CH_2$-$CH_3)$-$)_n$ and (-$CH_2CH(C(O)OH)$-$)_n$ [59]. The carbonyl compounds could be formed by the adsorption of CO and $CO_2$ on the catalyst surface [60]. The peaks around 286.00, 285.90, 285.80 and 285.90 eV are attributed to chain compounds primarily consisting of C-O bond for phenol ethers or alcohols [57]. The peaks around 284.40, 284.50 and 284.70 eV are ascribed to either graphitic carbon [61], or aliphatic and aromatic carbon polymers

[62,63]. Considering the morphology of the deposits observed by TEM, amorphous aliphatic and aromatic carbons are more likely to be formed.

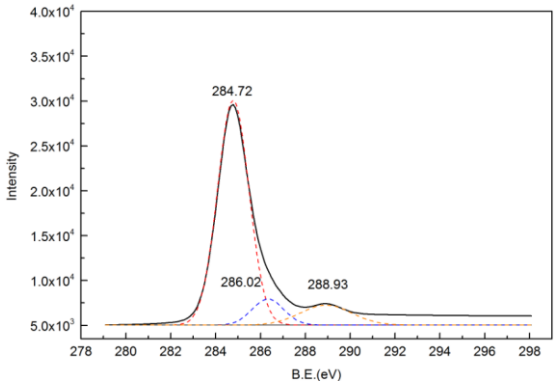


(a)

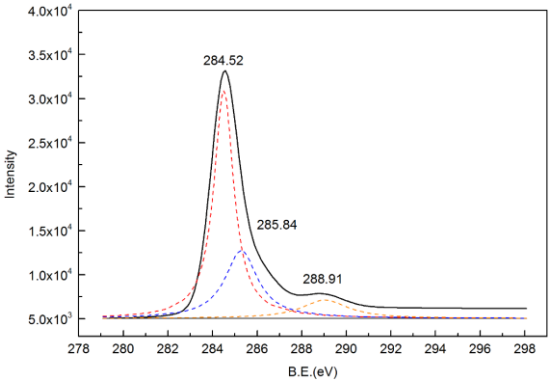


(b)

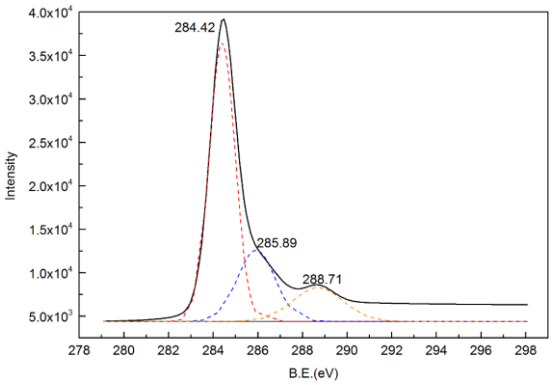


(c)

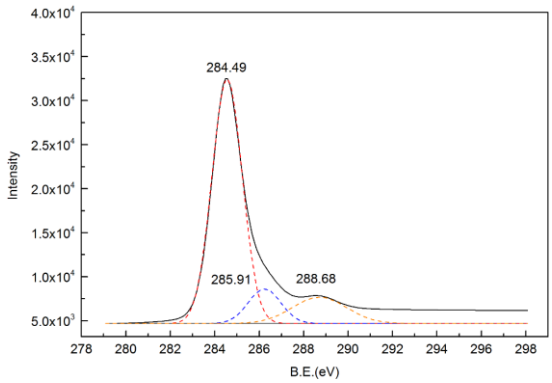


(d)

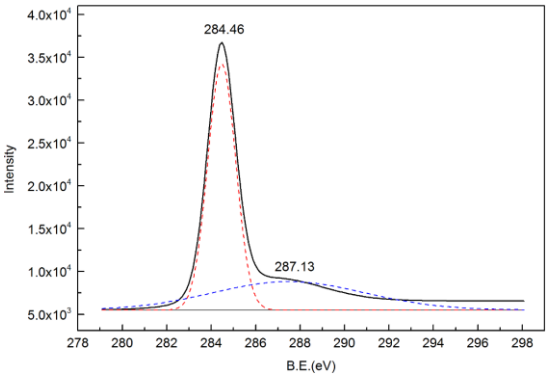


(e)

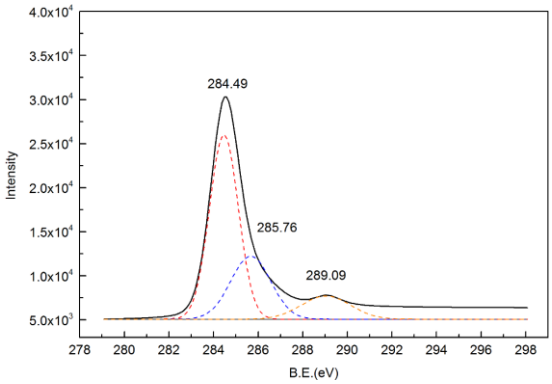


(f)

Fig. 9 XPS spectra of C(s1) for the spent catalyst: (a) 1%Ni/HZ(25) after D1, (b) 1%Ni/HZ(25) after D2, (c) 1%Ni/HZ(25) after D3, (d) 1%Co/HZ(25) after D6, (e) 1%Mo/HZ(25) after D7, (f) 1%Cu/HZ(25) after D10

In the case of the spent 1%Mo/HZ(25), apart from the peak at 284.46 eV representative of aliphatic and aromatic carbon, the other peak evolved at 287.13 eV is attributed to chain compounds containing metal carbide [64]. The signal for metal carbides compounds may also be related to peaks at 284 eV for the spent 1%Ni/HZ(25) [65] and 1%Co/HZ(25) [66], at 288 eV for 1%Co/HZ(25) [67], and at 289 eV for Cu/HZ(25) [68]. The metal carbides are known to be important intermediates in the formation of carbonaceous deposit [69].

The results shown in Fig. 9 reveal that the carbonaceous substance deposited on each spent metal/HZ(25) catalyst mainly consists of chain compounds of aliphatic carbon, aromatics and carbonyl groups, which can be attributed to the polycondensation of the methyl groups and aromatic compounds during the decomposition of anisole. Considering the experimental results in sections of 3.2 and 3.3, Phs and AHs can be the main precursors for the polycondensation reactions that originate from the metal carbides. The intensity of the three peaks for spent 1%Ni/HZ(25) increased with temperature, confirming the increment of temperature in the range of 400 to 600°C may result in larger carbon deposition. Regarding the four spent catalysts of different metal-based HZ(25) at 500°C, the spectra for the spent 1%Ni/HZ(25) and 1%Mo/HZ(25) catalysts showed the highest intensities peaks, which implies that these two catalysts are more prone to the formation of carbonaceous deposit compared to Co- and Cu-based catalysts. This result agrees with the experimental results on the higher catalytic activity of Ni/HZ(25) and Mo/HZ(25) compared to that of Co/HZ(25) and Cu/HZ(25).

### 3.6 Reaction pathways of catalytic deoxygenation in anisole decomposition over single metal/HZ(25)

Reaction pathways for the deoxygenation in the decomposition of anisole over metal/HZ(25) catalyst at 500°C are proposed based on the experimental investigation, as shown in Fig. 10.

The deoxygenation reactions follow transmethylation reactions as the second stage of anisole decomposition, and the products primarily consist of AHs, particularly targeting BTX compounds. The deoxygenation is regarded to occur with the involvement of hydrogen, i.e. hydrodeoxygenation (HDO). In this work, no hydrogen stream was input during the experiments, consequently, the hydrogen is assumed to be transferred in-situ during the reactions. The analyses of the gas products and spent catalyst showed the presence of alkanes and olefins potentially generated from methyl group polycondensation. Carbonaceous deposit of chain aliphatic and aromatic polymers was also observed, likely yielded from the polycondensation reactions of Phs and AHs. The polycondensation reactions could simultaneously produce abundant hydrogen, acting as reactant for the hydrodeoxygenation reactions occurring in the system.

Based on the results, three intrinsic reaction pathways are proposed for the deoxygenation reactions in the decomposition of anisole over metal/HZ(25) catalyst.

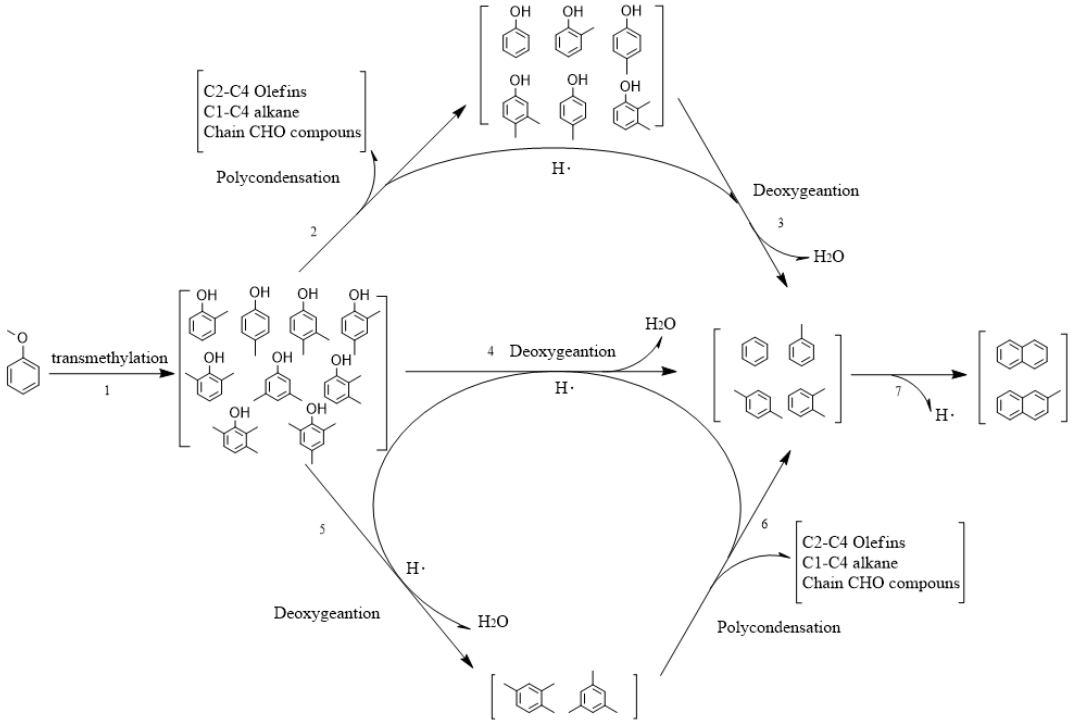


Fig. 10 Reaction pathways for catalytic deoxygenation during the decomposition process of anisole over x%M/HZ(25)

A phenolic compound could either undergo polycondensation prior to deoxygenation (pathway 2-3 in Fig. 10), or experience firstly deoxygenation followed by polycondensation (pathways 4 and 5-6). It should be noticed that xylenols and trimethyl phenols were obtained as low temperature products and only a little xylene and no trimethylbenzene were found in the products at 500°C. This implies that multi-methyl phenols may easily undergo demethylation reaction before deoxygenation or be more readily consumed in the polycondensation over the surface of metal/HZ(25).

The three pathways lead to the production of BTX, part of which could further be converted to PAH (naphthalene and methyl naphthalene, pathway 7), which were also observed in the liquid fraction along with the BTX products in most of the experiments.

# 4 Conclusion

In this work, the catalytic deoxygenation reaction during the decomposition of anisole over bi-functional catalyst was investigated. Experimental results showed that the increase in temperature favoured the increase in BTX yield and selectivity. However, it also increased the yield of undesirable carbonaceous deposits at the expense of both Phs and AHs compounds. 500˚C is found to be the optimum temperature for achieving the highest BTX yield and a moderate yield of carbonaceous deposit. The type of metal active site supported on HZ(25) was also found to have an influence on the BTX yield and selectivity. 1%Ni/HZ(25) presented the best selectivity towards the formation of BTX by converting more Phs to monocyclic AHs, while 1%Mo/HZ(25) presented the best catalytic activity towards high AHs production by impairing the formation of carbonaceous deposits. Both Ni and Mo based catalysts showed superior performance in BTX production compared to Co and Cu. Change of metal loading had significant influence in the case of x%Ni/HZ(25) series. Experiments based on 5%Ni/HZ(25) exhibited 98.7% BTX selectivity but with only 4.3 wt.% liquid yield, while 0.5%Ni/HZ(25) showed lower activity on the conversion of intermediates Phs into AHs. In the case of x%Mo/HZ(25), the loading ratio had less influence in the BTX yield and selectivity. The optimal loading ratio to produce BTX fraction was 1 wt.% both for the Ni- and Mo-based catalyst series. Carbonaceous deposit on spent catalysts consisted primarily of aliphatic and aromatic carbon produced by the polycondensation during the decomposition of anisole, and Phs and AHs were important precursor compounds. The deoxygenation was considered to proceed by the in-situ supply of hydrogen generated in the system by means of the polycondensation reactions.

# Author information

**Corresponding Authors**

D.S.: 101011398@seu.edu.cn

**Author Contributions**

All authors have given approval to the final version of the manuscript.

**Notes**

The authors declare no competing financial interest.

## Acknowledgement

The authors would like to acknowledge financial support from the National Natural Science Foundation of China (project references: 51476034 and 51628601), Natural Science Foundation of Jiangsu Province (project reference: BK20161423), and the FP7 Marie Curie iComFluid (project reference: 312261).

## References

[1] W. Boerjan, J. Ralph, M. Baucher, Lignin Biosynthesis, Annu. Rev. Plant Biol. 54 (2003) 519–546.

[2] C.S. Lancefield, N.J. Westwood, The synthesis and analysis of advanced lignin model polymers, Green Chem. 17 (2015) 4980–4990.

[3] W.J. Liu, H. Jiang, H.Q. Yu, Thermochemical conversion of lignin to functional materials: a review and future directions, Green Chem. 17 (2015) 4888–4907.

[4] A.V. Bridgwater, Review of fast pyrolysis of biomass and product upgrading, Biomass and Bioenergy. 38 (2012) 68–94.

[5] A.V. Bridgwater, G.V.C. Peacocke, Fast pyrolysis processes for biomass, Renew. Sustain. Energy Rev. 4 (2000) 1–73. http://www.scopus.com/inward/record.url?eid=2-s2.0-0033896848&partnerID=40&md5=0e406f0c2ff98f9795d0fec8732b9103.

[6] K.A. Jung, S.H. Woo, S.-R. Lim, J.M. Park, Pyrolytic production of phenolic compounds from the lignin residues of bioethanol processes, Chem. Eng. J. 259 (2015) 107–116.

[7] D.K. Shen, S. Gu, K.H. Luo, S.R. Wang, M.X. Fang, The pyrolytic degradation of wood-derived lignin from pulping process, Bioresour. Technol. 101 (2010) 6136–6146.

[8] S.J. Hurff, M.T. Klein, Reaction pathway analysis of thermal and catalytic lignin fragmentation by use of model compounds, Ind. Eng. Chem. Fundam. 22 (1983) 426–430.

[9] X. Zhu, R.G. Mallinson, D.E. Resasco, Role of transalkylation reactions in the conversion of anisole over HZSM-5, Appl. Catal. A Gen. 379 (2010) 172–181.

[10] J. Zhang, B. Fidalgo, D. Shen, R. Xiao, S. Gu, Mechanism of transmethylation in anisole decomposition over HZSM-5: Experimental study, J. Anal. Appl. Pyrolysis. 122 (2016) 323–331.

[11] X. Li, G. Chen, C. Liu, W. Ma, B. Yan, J. Zhang, Hydrodeoxygenation of lignin-derived bio-oil using molecular sieves supported metal catalysts: A critical review, Renew. Sustain. Energy Rev. 71 (2017) 296–308.

[12] Q. Meng, H. Fan, H. Liu, H. Zhou, Z. He, Z. Jiang, T. Wu, B. Han, Efficient Transformation of Anisole into Methylated Phenols over High-Silica HY Zeolites under Mild Conditions, ChemCatChem. 7 (2015) 2831–2835.

[13] T. Prasomsri, A.T. To, S. Crossley, W.E. Alvarez, D.E. Resasco, Catalytic conversion of anisole over HY and HZSM-5 zeolites in the presence of different hydrocarbon mixtures, Appl. Catal. B Environ. 106 (2011) 204–211.

[14] K. Wang, X. Dong, Z. Chen, Y. He, Y. Xu, Z. Liu, Highly selective synthesis of para-cresol by conversion of anisole on ZSM-5 zeolites, Microporous

304 Mesoporous Mater. 185 (2014) 61–65.

305 [15] J. Cornella, E. Gómez-Bengoa, R. Martin, Combined Experimental and
306 Theoretical Study on the Reductive Cleavage of Inert C–O Bonds with Silanes:
307 Ruling out a Classical Ni(0)/Ni(II) Catalytic Couple and Evidence for Ni(I)
308 Intermediates, J. Am. Chem. Soc. 135 (2013) 1997–2009.

309 [16] C. Mackie, R. Doolan, F. Nelson, Kinetics of the thermal decomposition of
310 methoxybenzene(anisole), J. Phys. Chem. C. 93 (1989) 664–670.

311 [17] Q. Song, F. Wang, J. Cai, Y. Wang, J. Zhang, W. Yu, J. Xu, Lignin
312 depolymerization (LDP) in alcohol over nickel-based catalysts via a
313 fragmentation–hydrogenolysis process, Energy Environ. Sci. 6 (2013) 994.

314 [18] M. Saidi, F. Samimi, D. Karimipourfard, T. Nimmanwudipong, B.C. Gates, M.R.
315 Rahimpour, Upgrading of lignin-derived bio-oils by catalytic hydrodeoxygenation,
316 Energy Environvironment Scicense. 7 (2014) 103–129.

317 [19] W. Mu, H. Ben, A. Ragauskas, Y. Deng, Lignin Pyrolysis Components and
318 Upgrading-Technology Review, Bioenergy Res. 6 (2013) 1183–1204.

319 [20] X. Zhu, L.L. Lobban, R.G. Mallinson, D.E. Resasco, Bifunctional transalkylation
320 and hydrodeoxygenation of anisole over a Pt/HBeta catalyst, J. Catal. 281 (2011)
321 21–29.

322 [21] R.C. Runnebaum, T. Nimmanwudipong, D.E. Block, B.C. Gates, Catalytic
323 conversion of compounds representative of lignin-derived bio-oils: a reaction
324 network for guaiacol, anisole, 4-methylanisole, and cyclohexanone conversion
325 catalysed by Pt/γ-Al2O3, Catal. Sci. Technol. 2 (2012) 113–118.

326 [22] J. Xiong, T. Kan, X. Li, T. Ye, Q. Li, Effects of Current upon Electrochemical
327 Catalytic Reforming of Anisole, Chinese J. Chem. Phys. 23 (2010) 693–700.

328 [23] M.A. González-Borja, D.E. Resasco, Anisole and Guaiacol Hydrodeoxygenation
329 over Monolithic Pt–Sn Catalysts, Energy & Fuels. 25 (2011) 4155–4162.

330 [24] S. Jin, Z. Xiao, C. Li, X. Chen, L. Wang, J. Xing, W. Li, C. Liang, Catalytic
331 hydrodeoxygenation of anisole as lignin model compound over supported nickel
332 catalysts, Catal. Today. 234 (2014) 125–132.

333 [25] E. Laurent, B. Delmon, Study of the hydrodeoxygenation of carbonyl, carboxylic
334 and guaiacyl groups over sulfided CoMo/γ-Al2O3 and NiMo/γ-Al2O3 catalyst,
335 Appl. Catal. A Gen. 109 (1994) 97–115.

336 [26] S. Mukundan, M. Konarova, L. Atanda, Q. Ma, J. Beltramini, Guaiacol
337 hydrodeoxygenation reaction catalyzed by highly dispersed, single layered MoS
338 2/C, Catal. Sci. Technol. 5 (2015) 4422–4432.

339 [27] T. Nimmanwudipong, R.C. Runnebaum, D.E. Block, B.C. Gates, Catalytic
340 Reactions of Guaiacol: Reaction Network and Evidence of Oxygen Removal in
341 Reactions with Hydrogen, Catal. Letters. 141 (2011) 779–783.

342 [28] C.R. Lee, J.S. Yoon, Y.W. Suh, J.W. Choi, J.M. Ha, D.J. Suh, Y.K. Park,
343 Catalytic roles of metals and supports on hydrodeoxygenation of lignin monomer
344 guaiacol, Catal. Commun. 17 (2012) 54–58.

345 [29] Q. Tan, G. Wang, A. Long, A. Dinse, C. Buda, J. Shabaker, D.E. Resasco,
346 Mechanistic analysis of the role of metal oxophilicity in the hydrodeoxygenation
347 of anisole, J. Catal. 347 (2017) 102–115.

348 [30] R. Shu, Y. Xu, L. Ma, Q. Zhang, P. Chen, T. Wang, Synergistic effects of highly
349 active Ni and acid site on the hydrodeoxygenation of syringol, Catal. Commun.
350 91 (2017) 1–5.

351 [31] A.L. Jongerius, R. Jastrzebski, P.C.A. Bruijnincx, B.M. Weckhuysen, CoMo
352 sulfide-catalyzed hydrodeoxygenation of lignin model compounds: An extended

353 reaction network for the conversion of monomeric and dimeric substrates, J.
354 Catal. 285 (2012) 315–323.

355 [32] I. Klein, B. Saha, M.M. Abu-Omar, Lignin depolymerization over Ni/C catalyst in
356 methanol, a continuation: effect of substrate and catalyst loading, Catal. Sci.
357 Technol. 5 (2015) 3242–3245.

358 [33] J. Horáček, F. Homola, I. Kubičková, D. Kubička, Lignin to liquids over sulfided
359 catalysts, Catal. Today. 179 (2012) 191–198.

360 [34] A. Toledano, L. Serrano, J. Labidi, A. Pineda, A.M. Balu, R. Luque,
361 Heterogeneously Catalysed Mild Hydrogenolytic Depolymerisation of Lignin
362 Under Microwave Irradiation with Hydrogen-Donating Solvents, ChemCatChem.
363 5 (2013) 977–985.

364 [35] K. Barta, T.D. Matson, M.L. Fettig, S.L. Scott, A. V. Iretskii, P.C. Ford, Catalytic
365 disassembly of an organosolv lignin via hydrogen transfer from supercritical
366 methanol, Green Chem. 12 (2010) 1640.

367 [36] R. Thilakaratne, J.-P. Tessonnier, R.C. Brown, Conversion of methoxy and
368 hydroxyl functionalities of phenolic monomers over zeolites, Green Chem. 18
369 (2016) 2231–2239.

370 [37] S. Ivanova, B. Louis, B. Madani, J.P. Tessonnier, M.J. Ledoux, C. Pham-Huu,
371 ZSM-5 coatings on-SiC monoliths: Possible new structured catalyst for the
372 methanol-to-olefins process, J. Phys. Chem. C. 111 (2007) 4368–4374.

373 [38] M. Guisnet, J.P. Gilson, Zeolites for Cleaner Technologies, Imperial College
374 Press, 2002.

375 [39] A.R. Ardiyanti, S.A. Khromova, R.H. Venderbosch, V.A. Yakovlev, H.J. Heeres,
376 Catalytic hydrotreatment of fast-pyrolysis oil using non-sulfided bimetallic Ni-Cu
377 catalysts on a δ-Al2O3 support, Appl. Catal. B Environ. 117–118 (2012) 105–

117.

[40] S.A. Khromova, A.A. Smirnov, O.A. Bulavchenko, A.A. Saraev, V. V. Kaichev, S.I. Reshetnikov, V.A. Yakovlev, Anisole hydrodeoxygenation over Ni–Cu bimetallic catalysts: The effect of Ni/Cu ratio on selectivity, Appl. Catal. A Gen. 470 (2014) 261–270.

[41] S. Pichaikaran, P. Arumugam, Vapour phase hydrodeoxygenation of anisole over ruthenium and nickel supported mesoporous aluminosilicate, Green Chem. 18 (2016) 2888–2899.

[42] I.T. Ghampson, G. Pecchi, J.L.G. Fierro, A. Videla, N. Escalona, Catalytic hydrodeoxygenation of anisole over Re-MoO x /TiO 2 and Re-VO x /TiO 2 catalysts, Appl. Catal. B Environ. 208 (2017) 60–74.

[43] H.S. Fogler, Chemical reactors, in: Chem. React., Washington, D.C. : American Chemical Society, 1981. http://www.essentialchemicalindustry.org/processes/chemical-reactors.html.

[44] T.M. Sankaranarayanan, A. Berenguer, C. Ochoa-Hernández, I. Moreno, P. Jana, J.M. Coronado, D.P. Serrano, P. Pizarro, Hydrodeoxygenation of anisole as bio-oil model compound over supported Ni and Co catalysts: Effect of metal and support properties, Catal. Today. 243 (2015) 163–172.

[45] Z.Y. Zakaria, J. Linnekoski, N.A.S. Amin, Catalyst screening for conversion of glycerol to light olefins, Chem. Eng. J. 207–208 (2012) 803–813.

[46] C. Ochoa-Hernández, Y. Yang, P. Pizarro, V.A. De La Peña O'Shea, J.M. Coronado, D.P. Serrano, Hydrocarbons production through hydrotreating of methyl esters over Ni and Co supported on SBA-15 and Al-SBA-15, Catal. Today. 210 (2013) 81–88.

[47] H. Liu, Y. Xu, H2-TPR Study on Mo/HZSM-5 Catalyst for CH4

403 Dehydroaromatization, Chinese J. Catal. 27 (2006) 319–323.

404 [48] A. Martínez, E. Peris, Non-oxidative methane dehydroaromatization on
405 Mo/HZSM-5 catalysts: Tuning the acidic and catalytic properties through partial
406 exchange of zeolite protons with alkali and alkaline-earth cations, Appl. Catal. A
407 Gen. 515 (2016) 32–44.

408 [49] L. Li, J. Chen, S. Zhang, N. Guan, M. Richter, R. Eckelt, R. Fricke, Study on
409 metal-MFI/cordierite as promising catalysts for selective catalytic reduction of
410 nitric oxide by propane in excess oxygen, J. Catal. 228 (2004) 12–22.

411 [50] C. Torreabreu, M. Ribeiro, C. Henriques, G. Delahay, NO TPD and H2-TPR
412 studies for characterisation of CuMOR catalysts The role of Si/Al ratio, copper
413 content and cocation, Appl. Catal. B Environ. 14 (1997) 261–272.

414 [51] A. Martínez, C. López, F. Márquez, I. Díaz, Fischer–Tropsch synthesis of
415 hydrocarbons over mesoporous Co/SBA-15 catalysts: the influence of metal
416 loading, cobalt precursor, and promoters, J. Catal. 220 (2003) 486–499.

417 [52] O. González, H. Pérez, P. Navarro, L.C. Almeida, J.G. Pacheco, M. Montes, Use
418 of different mesostructured materials based on silica as cobalt supports for the
419 Fischer–Tropsch synthesis, Catal. Today. 148 (2009) 140–147.

420 [53] C. Cheng, D. Shen, R. Xiao, C. Wu, Methanation of syngas (H2/CO) over the
421 different Ni-based catalysts, Fuel. 189 (2017) 419–427.

422 [54] R. Watanabe, Y. Hondo, K. Mukawa, C. Fukuhara, E. Kikuchi, Y. Sekine, Stable
423 and selective perovskite catalyst for dehydrogenation of propane working with
424 redox mechanism, J. Mol. Catal. A Chem. 377 (2013) 74–84.

425 [55] J.W. Chai, J.S. Pan, S.J. Wang, C.H.A. Huan, G.S. Lau, Y.B. Zheng, S. Xu,
426 Thermal behaviour of ultra-thin Co overlayers on rutile TiO2(100) surface, Surf.
427 Sci. 589 (2005) 32–41.

[56] M. Domínguez, E. Taboada, H. Idriss, E. Molins, J. Llorca, Fast and efficient hydrogen generation catalyzed by cobalt talc nanolayers dispersed in silica aerogel, J. Mater. Chem. 20 (2010) 4875.

[57] Y. Li, C. Zhang, Y. Liu, S. Tang, G. Chen, R. Zhang, X. Tang, Coke formation on the surface of Ni/HZSM-5 and Ni-Cu/HZSM-5 catalysts during bio-oil hydrodeoxygenation, Fuel. 189 (2017) 23–31.

[58] B. Rahzani, M. Saidi, H.R. Rahimpour, B.C. Gates, M.R. Rahimpour, Experimental investigation of upgrading of lignin-derived bio-oil component anisole catalyzed by carbon nanotube-supported molybdenum, RSC Adv. 7 (2017) 10545–10556.

[59] X. Zou, T. Chen, H. Liu, P. Zhang, D. Chen, C. Zhu, Catalytic cracking of toluene over hematite derived from thermally treated natural limonite, Fuel. 177 (2016) 180–189.

[60] B.S. Liu, L. Jiang, H. Sun, C.T. Au, XPS, XAES, and TG/DTA characterization of deposited carbon in methane dehydroaromatization over Ga–Mo/ZSM-5 catalyst, Appl. Surf. Sci. 253 (2007) 5092–5100.

[61] B.M. Weckhuysen, M.P. Rosynek, J.H. Lunsford, Characterization of surface carbon formed during the conversion of methane to benzene over Mo/H-ZSM-5 catalysts, Catal. Letters. 52 (1998) 31–36.

[62] P. Albers, K. Seibold, T. Haas, G. Prescher, W.F. Hölderich, SIMS/XPS Study on the Deactivation and Reactivation of B-MFI Catalysts Used in the Vapour-Phase Beckmann Rearrangement, J. Catal. 176 (1998) 561–568.

[63] H. Hantsche, High resolution XPS of organic polymers, the scienta ESCA300 database. By G. Beamson and D. Briggs, Wiley, Chichester 1992, 295 pp., hardcover, £ 65.00, ISBN 0-471-93592-1, Adv. Mater. 5 (1993) 778–778.

[64] H. Willemen, L.F. Wuyts, D.F. van de Vondel, G.P. van der Kelen, ESCA and IR study of cyclopentadienyl tungsten and molybdenum carbonyl compounds, J. Electron Spectros. Relat. Phenomena. 11 (1977) 245–250.

[65] D.H. Karweik, N. Winograd, Nitrogen Charge Distribution in Free-Base Porphyrins, Metalloporphyrins, and their reduced analogues observed by X-ray Photoelectron Spectroscopy, Inorg. Chem. 15 (1976) 2336–2342.

[66] M. Barber, J.A. Connor, L.M.R. Derrick, M.B. Hall, I.H. Hillier, High energy photoelectron spectroscopy of transition metal complexes. Part 2.—Metallocenes, J. Chem. Soc. Faraday Trans. 2 Mol. Chem. Phys. 69 (1973) 559–562.

[67] D.L. Hoof, D.G. Tisley, R.A. Walton, Studies on metal carboxylates. Part III. Pyridine-2,6-dicarboxylates of the lanthanides. Synthesis and spectral studies and the X-ray photoelectron spectra of several pyridine carboxylate complexes, J. Chem. Soc. Dalt. Trans. (1973) 200.

[68] G. Moretti, G. Fierro, M. Lo Jacono, P. Porta, Characterization of CuO-ZnO catalysts by X-ray photoelectron spectroscopy: Precursors, calcined and reduced samples, Surf. Interface Anal. 14 (1989) 325–336.

[69] B.J. Cooper, D.L. Trimm, Carbon Deposition from Propylene on Polycrystalline and Single-Crystal Iron, J. Catal. 62 (1980) 35–43.

https://dspace.org/

# Mechanism of deoxygenation in anisole decomposition over single-metal loaded HZSM-5: Experimental study

**Zhang, Jiajun; Fidalgo, Beatriz; Kolios, Athanasios; Shen, Dekui; Gu, Sai**

**2017-11-20**
Elsevier
https://doi.org/10.1016/j.cej.2017.11.128
Jiajun Zhang, Beatriz Fidalgo, Athanasios Kolios, et.al., Mechanism of deoxygenation in anisole decomposition over single-metal loaded HZSM-5: Experimental study. Chemical Engineering Journal, Volume 336, 15 March 2018, Pages 211-222

Downloaded from a DSpace repository. https://dspace.org/